Available online at www.sciencedirect.com
SCIENCE DIRECT®
International Journal of Heat and Mass Transfer 47 (2004) 4125–4136
International Journal of HEAT and MASS TRANSFER
www.elsevier.com/locate/ijhmt

Experimental heat transfer coefficients during refrigerant vaporisation and condensation inside herringbone-type plate heat exchangers with enhanced surfaces

G.A. Longo [a,*], A. Gasparella [a], R. Sartori [b]

[a] Department of Management and Engineering, University of Padova, Stradella S. Nicola 3, I-36100 Vicenza, Italy
[b] Onda S.p.A. Via Baden Powel 11, I-36045 Lonigo (VI), Italy

Received 6 November 2003; received in revised form 7 May 2004
Available online 26 June 2004

Abstract

This paper presents the experimental work carried out to apply "cross-grooved" surfaces to refrigerant vaporisation and condensation inside plate heat exchangers (PHE) with herringbone macro-scale corrugation. This paper also investigates the effect of an increase in the surface roughness of the plate on refrigerant two-phase heat transfer inside PHE. The enhanced surfaces are experimentally evaluated both in vaporisation and condensation tests with refrigerant 22, and compared against a PHE with a smooth surface. The experimental results show that the "cross-grooved" surface is useful both in vaporisation and condensation, whereas the increase in surface roughness is useful only in vaporisation. The "cross-grooved" surface gives an increase in the heat transfer coefficient from 30% to 40% in vaporisation to 60% in condensation with respect to a PHE with a smooth surface. The enhancement in heat transfer coefficient is higher than the simple increase in heat transfer surface area. A fair agreement was found between present experimental data and semi-empirical correlations both for condensation and vaporisation inside PHE.

1. Introduction

Plate heat exchangers (PHE) are commonly used for single-phase heat transfer from liquid to liquid having extensive application in the pharmaceutical industry, chemical processing and food treatment. In the last 20 years they have also been used for two-phase heat transfer, particularly as evaporators and condensers in chillers and heat pumps. The application to high pressure refrigerant fluids required the development of a new type of PHE, the brazed plate heat exchangers (BPHE), in which the different plates are brazed and not linked by gaskets. Although ensuring a great mechanical resistance, this solution seemed to be in the past incompatible with the application of micro-finned surfaces, which are particularly effective in two-phase heat transfer with refrigerant, as the enhanced surfaces might be filled by the soldering material. Therefore the BPHE commercially available today present smooth heat transfer surface with macro-scale corrugations (washboard, herringbone, etc.), which are suitable only for single-phase heat transfer and not specifically developed for two-phase applications. New soldering techniques, such as laser for example, permit applying enhanced surfaces on the refrigerant side to increase condensation and vaporisation heat transfer.

In open literature, it is possible to find several works on traditional PHE in single-phase applications, whereas works on BPHE in refrigeration applications are relatively scarce. Tonon et al. [1] and Palm and Tonon [2] presented good reviews on the thermal and hydraulic performances of plate heat exchangers in refrigerant condensation and vaporisation. More recently Yan and Lin [3,4] experimentally investigated the effects of mean vapour quality, mass flux, heat flux and pressure on heat

* Corresponding author. Tel.: +39-0444-998726; fax: +39-0444-998888.
E-mail address: tony@gest.unipd.it (G.A. Longo).

0017-9310/$ - see front matter © 2004 Elsevier Ltd. All rights reserved.
doi:10.1016/j.ijheatmasstransfer.2004.05.001

Nomenclature

A	nominal area of a plate, m^2
b	height of the corrugation or the fins, m
c_p	specific heat capacity, $J\,kg^{-1}\,K^{-1}$
c_w	correction term in Eq. (11)
d_h	hydraulic diameter, m
F	correction term in Eq. (11)
G	mass flux, $kg\,m^{-2}\,s^{-1}$
h	heat transfer coefficient, $W\,m^{-2}\,K^{-1}$
J	specific enthalpy, $J\,kg^{-1}$
L	flow length of the plate from centre of inlet port to centre of exit port, m
m	mass flow rate, $kg\,s^{-1}$
M	molecular weight, $kg\,kmol^{-1}$
N	number of effective plates
p	pitch of the corrugation or the fins, m
P	pressure, Pa
Pr	Prandtl number, $Pr = \mu c_p/\lambda$,
q	heat flux, $W\,m^{-2}$
Q	heat flow rate, W
R_a	arithmetic mean roughness (ISO 4271/1), μm
R_p	roughness (DIN 4762/1), μm
Re	Reynolds number, $Re = Gd_h/\mu$
S	nominal heat transfer area, m^2
s	plate wall thickness, m
T	temperature, K
U	overall heat transfer coefficient, $W\,m^{-2}\,K^{-1}$
W	width of the plate, m
x	vapour quality
X	co-ordinate in Fig. 7 (Eq. (7))
Y	co-ordinate in Fig. 7 (Eq. (8))

Greek symbols

β	inclination angle of the corrugation, °
Δ	difference
ϕ	ratio between finned and smooth surface area
λ	thermal conductivity, $W\,m^{-1}\,K^{-1}$
μ	viscosity, $kg\,m^{-1}\,s^{-1}$
ρ	density, $kg\,m^{-3}$

Subscripts

cr	critical
E	external channel
I	internal channel
L	liquid phase
ln	logarithmic
m	average
p	plate
r	refrigerant
s	saturation
sub	subcooling
sup	superheating
v	vapour phase
w	water
wi	water inlet
wo	water outlet
0	reference conditions in Eq. (11)

transfer and pressure drop during vaporisation and condensation of refrigerant R134a inside a plate heat exchanger. They also presented empirical correlations for heat transfer coefficient and friction factor based on their experimental data. Hsieh and Lin [5] reported experimental data on boiling heat transfer and pressure drop of refrigerant R410A in a plate heat exchanger. The effects of mean vapour quality, mass flux, heat flux and pressure were evaluated and empirical correlations were proposed for heat transfer coefficient and friction factor. Matsushita and Ucida [6] presented experimental data relative to vaporisation of refrigerant R22 inside a PHE with special plates embossed with pyramid-like structures. These new plates gave a vaporisation heat transfer coefficient 50–100% higher than traditional herringbone-type plates and a similar pressure drop on the refrigerant side.

The present paper describes the experimental work carried out to apply micro-finned surfaces to refrigerant condensation and vaporisation inside a herringbone-type PHE. This paper also investigates the effect of an increase in the surface roughness of the plate on refrigerant two-phase heat transfer inside PHE. The enhanced surfaces are experimentally evaluated both in vaporisation and condensation tests with refrigerant 22 and compared against a PHE with smooth surface. The experimental heat transfer coefficients are compared against semi-empirical correlations.

2. Enhanced surfaces

The most widespread enhanced surfaces for refrigerant two-phase heat transfer inside tubes are "micro-fin" and "cross-grooved" as they ensure a greater improvement in heat transfer with a small penalty in pressure drop. Typical "micro-fin" surfaces present a single set of rectangular or trapezoidal micro-grooves with a depth ranging from 0.1 to 0.25 mm, a pitch from 0.4 to 0.5 mm and a spiral angle (inclination with respect to the flow direction) from 10° to 30°. The "cross-grooved" surfaces present an additional set of grooves at

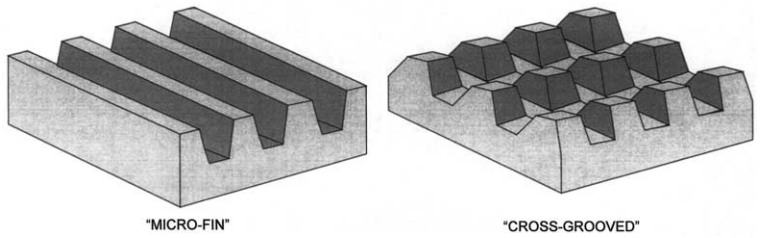

Fig. 1. Typical configuration of ''micro-fin'' and ''cross-grooved'' surfaces.

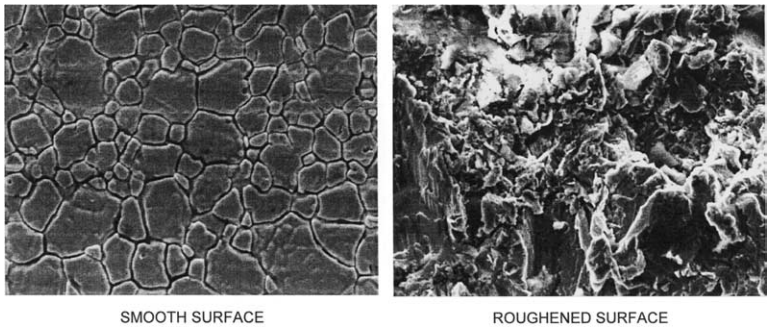

Fig. 2. Smooth and roughened surfaces at the scanning electron microscope (×1200).

the same spiral angle, but in opposite angular direction to the first set with equal or different groove depth. The intersection between the two sets of grooves produces a regular distribution of pin fins. Fig. 1 shows the typical configuration of ''micro-fin'' and ''cross-grooved'' surfaces. The ''micro-fin'' tubes show a heat transfer enhancement, with respect to the equivalent smooth tubes, ranging from 80% to 180% in refrigerant vaporisation and condensation, with a pressure loss increase from 20% to 80%. ''Cross-grooved'' tubes give heat transfer performance 25–30% higher than ''micro-fin'' tubes with a pressure drop only 6–10% higher both in vaporisation and condensation. Heat transfer and pressure drop enhancements are partly due to the simple increase in the effective exchange area and also to the turbulence induced in the liquid film by the micro-fins and to the surface tension effect on the liquid drainage, and moreover (in vaporisation) to the increase in the nucleation site density in the interfin spaces. In [7] it is possible to find a detailed analysis of heat transfer inside enhanced tubes during refrigerant vaporisation and condensation. The ''cross-grooved'' surface seems to be the most interesting enhanced surface for refrigerant condensation and vaporisation inside tube.

The primary aim of this work is to investigate the application of the ''cross-grooved'' surface into herringbone-type PHE for refrigerant vaporisation and condensation.

Several experimental works [8–10] on refrigerant vaporisation inside PHE show that nucleate boiling is the dominant heat transfer regime. This regime is greatly

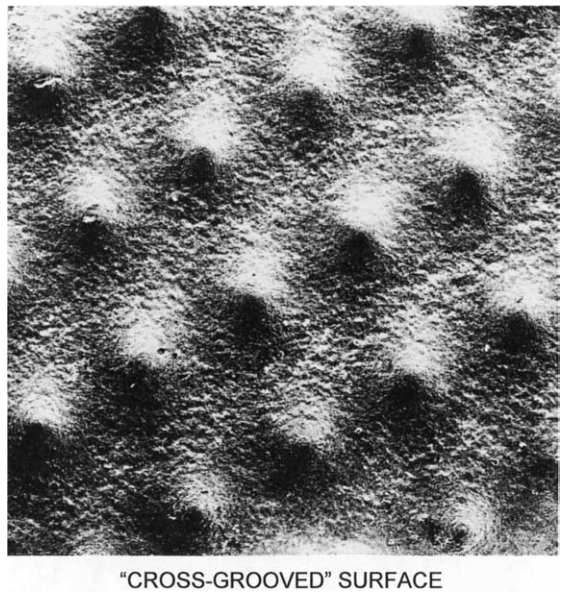

Fig. 3. ''Cross-grooved'' surface at the scanning electron microscope (×40).

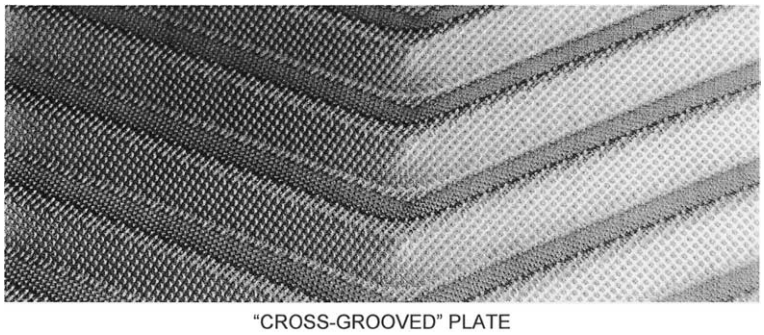

Fig. 4. Photo of the "cross-grooved" plate.

affected by the surface roughness which increases the nucleation site density. Therefore the present work also investigates the effect of an increase in the surface roughness of the plate on refrigerant condensation and vaporisation inside herringbone-type PHE.

The heat transfer performances of the different surfaces are compared in vaporisation and condensation tests with refrigerant 22 inside PHE. Three different prototypes have been realised: the reference prototype with smooth surface, the roughened prototype and the "cross-grooved" prototype. All the prototypes present the same macro-scale herringbone corrugation with an inclination angle of 65°, a corrugation amplitude of 2 mm, a corrugation pitch of 8 mm, whereas they have a different surface configuration. The arithmetic mean roughness R_a of the reference smooth prototype is 0.4 μm, whereas the roughened prototype presents a roughness R_a of 3.6 μm. The "cross-grooved" prototype

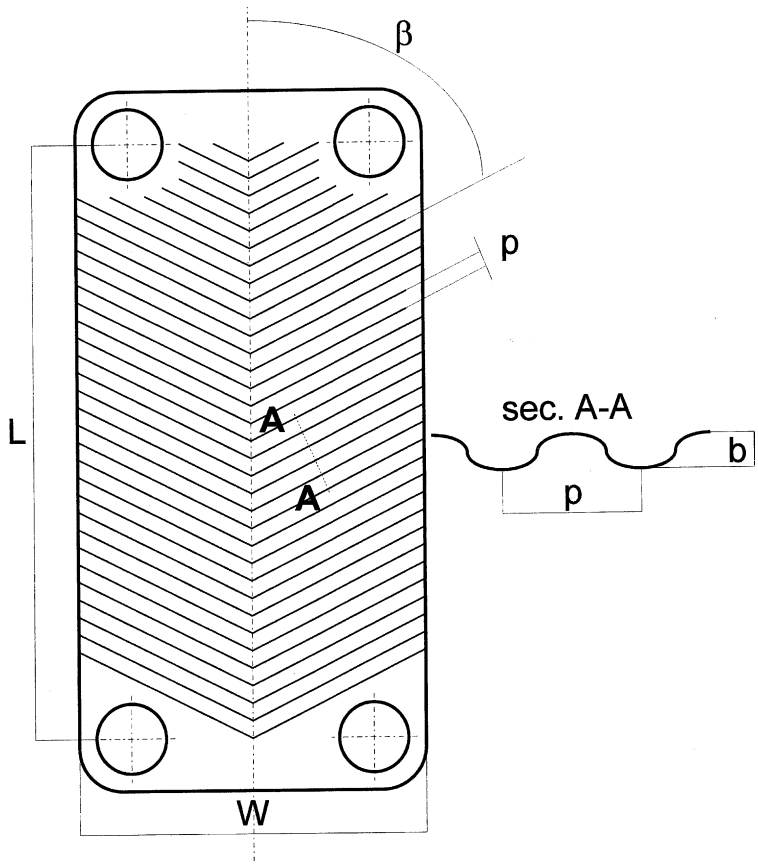

Fig. 5. Schematic view of the plate.

Table 1
Geometrical characteristics of the prototypes

Fluid flow plate length L (mm)	290
Plate width W (mm)	75
Nominal area of the plate A (m^2)	0.02175
Enlargement factor of the corrugation	1.24
Corrugation type	Herringbone
Angle of the corrugation β (°)	65
Corrugation amplitude b (mm)	2
Corrugation pitch p (mm)	8
Number of plates	4
Number of channels on refrigerant side	1
Number of channels on water side	2
Reference prototype roughness (μm)	0.4
Roughened prototype roughness (μm)	3.6
Micro-groove depth (mm)	0.05
Micro-groove width (mm)	0.2
Micro-groove pitch (mm)	0.5
Inclination angle of the micro-groove (°)	45
Number of micro-groove sets	2

presents a surface with two sets of rectangular micro-grooves with a depth of 0.05 mm, a width of 0.2 mm, a pitch of 0.5 mm and an inclination angle of 45°.

Fig. 2 shows the comparison between the smooth and the roughened surface at the scanning electron microscope (×1200): the roughened surface presents numerous cavities providing more and larger sites for bubble growth than the smooth surface. Fig. 3 shows a photo at the scanning electron microscope (×40) of the "cross-grooved" surface, whereas Fig. 4 shows a photo of the "cross-grooved" plate: the regular distribution of pin fins is easily recognisable.

Each prototype consists of four plates and presents two channels on the water side (external channels) and a single channel on the refrigerant side (internal channel) to prevent an uneven distribution of the refrigerant in the channels. It is well known that an uneven distribution of the refrigerant has a large influence on the performance of PHE: therefore the results obtained on a single refrigerant channel are useful only for comparison between different surfaces.

The prototypes have been assembled using frame plates and perimetrical welding to avoid the adhesion of the brazing material to the heat transfer surface.

Fig. 5 and Table 1 show the main geometrical characteristics of all the different prototypes.

3. Experimental set-up

The above prototypes have been evaluated in an experimental rig for the measurement of the heat transfer coefficient during refrigerant condensation and vaporisation. The experimental facility, shown in Fig. 6, consists of a refrigerant loop, a cooling water loop and a refrigerated water loop.

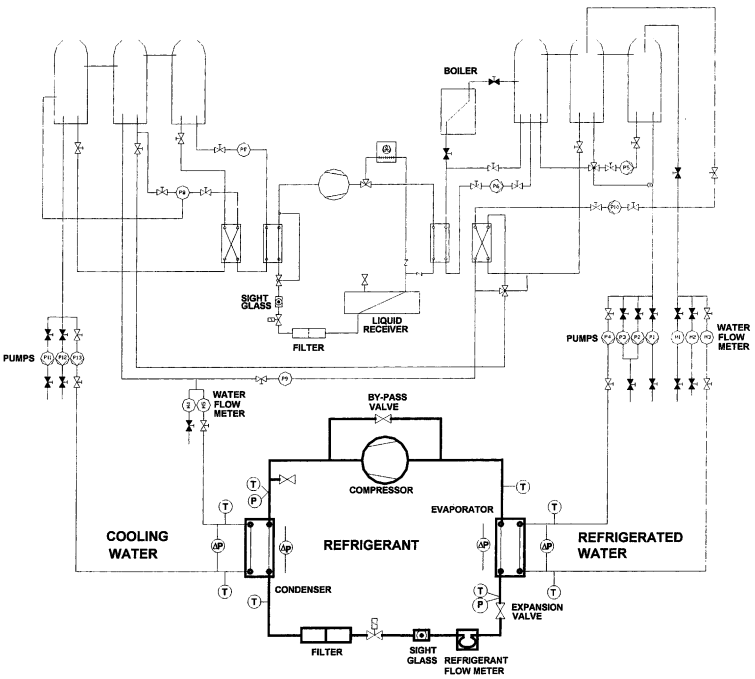

Fig. 6. Schematic view of the experimental test rig.

The first loop is a traditional chiller with a hermetic compressor and a manual throttling valve in which the condenser and the evaporator, supplied respectively with the cooling water and the refrigerated water, can be tested. The refrigerant mass flow rate is controlled by the throttling valve and a by-pass valve of the hot-gas compressor. The refrigerant loop has no lubricant oil separator in order to reproduce the real operating conditions inside a vapour compression chiller in which the refrigerant flow is contaminated by lubricant oil in a variable percentage from 1% to 3%.

The refrigerated water loop is able to supply a water flow at a temperature variable from 3 to 15 °C with a stability within ±0.1 K, whereas the cooling water loop is able to supply a water flow at a temperature variable from 15 to 35 °C with a stability within ±0.1 K.

The refrigerant temperatures at the inlet and outlet of the condenser and the evaporator are measured by platinum resistance thermometers Pt100 having an accuracy within ±0.1 K. The refrigerant pressures at the inlet of the condenser and the evaporator are measured by strain-gage pressure transducers, having an accuracy within 0.075% f.s., whereas the pressure drops through evaporator and condenser are measured by strain-gage differential pressure transducers having an accuracy within 0.075% f.s. The refrigerant mass flow rate is measured by means of a Coriolis effect mass flow meter having an accuracy of 0.1% of the measured value. The absolute atmospheric pressure is measured by a barometer having an accuracy of 0.08% f.s.

The refrigerated water and the cooling water mass flow rates are measured by means of a Coriolis effect mass flow meter having an accuracy of 0.1% of the measured value. The temperatures of the cooling water and the refrigerated water at the inlet and the outlet of the condenser and the evaporator respectively are measured by platinum resistance thermometers Pt 100 having an accuracy within ±0.1 K. The pressure drops on the water side of the condenser and the evaporator are measured by strain-gage differential pressure transducers having an accuracy within 0.075% f.s. All the measurements are scanned and recorded by a data logger linked to a P.C. Table 2 shows the main features of the different measuring devices in the experimental rig.

4. Data reduction

The overall heat transfer coefficient U is equal to the ratio between the heat flow rate exchanged Q and the nominal heat transfer area S and the logarithmic mean temperature difference $\Delta T_{\ln}$:

$$U = Q/(S\Delta T_{\ln}) \tag{1}$$

The heat flow rate exchanged is derived from a thermal balance on the water side:

$$Q = m_{\mathrm{w}} c_{p\mathrm{w}} \Delta T_{\mathrm{w}} \tag{2}$$

where m_{w} is the water mass flow rate measured by the Coriolis mass flow meter, $c_{p\mathrm{w}}$ is the water specific heat capacity and ΔT_{w} is the temperature variation on the water side derived from the temperature measurements. The thermal balance on the water side is compared with the thermal balance on the refrigerant side:

$$Q_{\mathrm{r}} = m_{\mathrm{r}} \Delta J_{\mathrm{r}} \tag{3}$$

where m_{r} is the refrigerant mass flow rate measured by the Coriolis mass flow meter and ΔJ_{r} is the enthalpy variation on the refrigerant side derived from the temperature and pressure measurements. Each test is acceptable only if the difference between the thermal balance on the water side and the refrigerant side is less than 3%.

The nominal heat transfer area:

$$S = NA \tag{4}$$

is equal to the nominal projected area $A = L \times W$ of the single plate multiplied by the number N of the effective elements in heat transfer, as suggested by Shah and Focke [11]. The logarithmic mean temperature difference is equal to:

$$\Delta T_{\ln} = [(T_{\mathrm{wo}} - T_{\mathrm{wi}})/\ln[(T_{\mathrm{s}} - T_{\mathrm{wo}})/(T_{\mathrm{s}} - T_{\mathrm{wi}})] \tag{5}$$

where T_{s} is the saturation temperature of the refrigerant derived from the mean vapour pressure measured on refrigerant side, T_{wi} and T_{wo} the water temperatures at the inlet and the outlet of the heat exchanger measured by the platinum resistance thermometers Pt100. The logarithmic mean temperature difference is computed with reference to the saturation temperature on the

Table 2
Specification of the different measuring devices

Devices	Type	Accuracy	Range
Thermometers	Pt100	0.1 K	−100/+500 °C
Refrigerant flow meters	Coriolis effect	0.1%	0–180 kg/h
Water flow meters	Coriolis effect	0.1%	0–360 kg/h
Refrigerant pressure transducers	Strain-gage	0.075% f.s.	0–2.0 MPa
Differential pressure transducers	Strain-gage	0.075% f.s.	0–186 kPa
Barometer	Strain-gage	0.080% f.s.	80–120 kPa

refrigerant side without taking into account any subcooling or superheating on the refrigerant side as is usual in the design procedure. This assumption does not affect the results of the comparison between the different surfaces, as all the tests were carried out under the same superheating and subcooling.

The heat transfer coefficients on the refrigerant side h_r were derived from the global heat transfer coefficient U:

$$h_r = (1/U - s/\lambda_p - 1/h_w)^{-1} \quad (6)$$

by computing the water side heat transfer coefficient h_w using a modified Wilson plot technique. A specific set of experimental runs consisting of more than 40 water-to-water tests was carried out on the prototype with smooth surface to determine the calibration correlation for heat transfer on the water side in accordance with Muley and Manglick [12]. This modification of the classical Wilson plot technique incorporates an account of variable fluid property effects: Fig. 7 shows the water-to-water data plotted on the co-ordinates:

$$X = (\lambda_I/\lambda_E)(Re_I/Re_E)^{0.66}(Pr_I/Pr_E)^{0.333} \quad (7)$$

$$Y = (1/U - s/\lambda_p)[(\lambda_I/d_h)(Re_I)^{0.66}Pr_I^{0.333}] \quad (8)$$

where subscripts I and E refer to the internal channel and to the external channels of the prototype tested.

The slope of the plot gives the constant in the calibration correlation, a power-law type, for heat transfer coefficients on the water side. The exponent on Reynolds number $n = 0.66$ was derived by a best fitting procedure on the experimental data. The calibration correlation for water side heat transfer coefficient is:

$$h_w = 0.46(\lambda_w/d_h)Re_w^{0.66}Pr_w^{0.333} \quad 350 < Re_w < 1100 \quad 5 < Pr_w < 10 \quad (9)$$

It has to be noted that Eq. (9) is only a calibration equation for the present test facility, valid only over the limited range of present water-to-water data.

The refrigerant properties are evaluated by Refprop 6.1 (Nist 2001 [13]). A detailed error analysis performed in accordance with [14] indicates an overall accuracy within 12% for the refrigerant heat transfer coefficient measurement.

5. Analysis of the results

Two different series of experimental tests were carried out with refrigerant 22: the first included 58 vaporisation runs, the second 24 condensation runs. In the vaporisation tests, the upflow of boiling refrigerant 22 in the central channel received heat from the downflow of refrigerated water in the other two channels. In the condensation tests, the downflow of condensing refrigerant 22 in the central channel released heat to the upflow of cooling water in the other two channels. During the vaporisation runs, the water inlet temperature T_{wi} was set at 12 °C with a temperature decrease on the water side of 5 °C, whereas on the refrigerant side the inlet vapour quality ranged from 0.16 to 0.21 with an outlet superheating ΔT_{sup} around 4–5 °C. In the condensation runs, the water inlet temperature T_{wi} was set at 30 °C with a water temperature gain of 5 °C and a subcooling on the refrigerant side at the outlet of the condenser ΔT_{sub} around 4–5 °C. The operating conditions of present experimental data are typical for air conditioning chillers cooled by a cooling tower. Table 3 shows the main operating conditions under experimental tests: refrigerant saturation temperature T_s, water inlet T_{wi} and outlet T_{wo} temperatures, refrigerant superheating ΔT_{sup} during vaporisation tests and subcooling ΔT_{sub} during condensation tests, inlet vapour quality x_i during

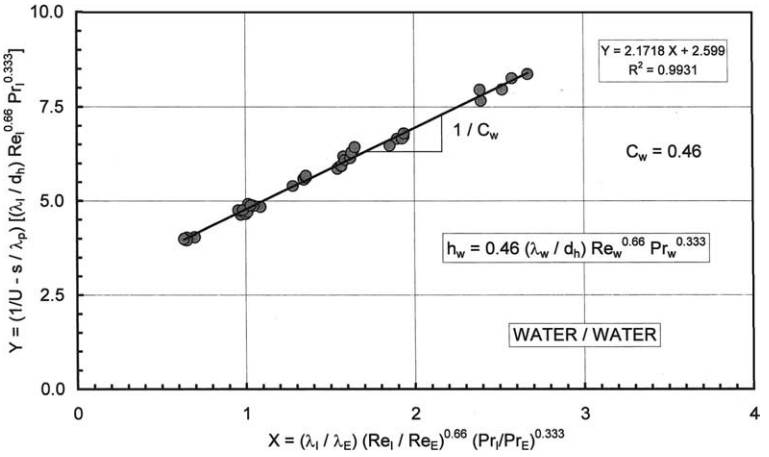

Fig. 7. Modified Wilson plot results for calibration of water side heat transfer coefficient.

Table 3
Operating conditions during experimental tests

Test	Runs	T_s (°C)	$\Delta T_{sup/sub}$ (°C)	x_i	T_{wi} (°C)	T_{wo} (°C)	G_r (kg m^{-2} s^{-1})	G_w (kg m^{-2} s^{-1})	Q/S (kW m^{-2})
Vaporisation	58	1.2–3.2	4.0–5.0	0.16–0.21	12.0	7.0	25.5–36.3	98.6–150.9	14.7–21.9
Condensation	24	39.5–44.4	4.0–5.0	=	30.0	35.0	23.5–40.9	109.7–194.5	15.8– 27.8
Maximum uncertainty	=	±0.1 K	±0.2 K	±0.03	±0.1 K	±0.1 K	±0.1%	±0.1%	±4%

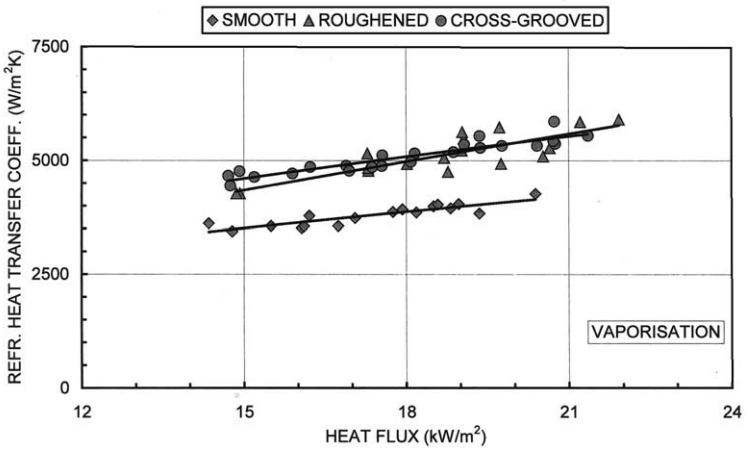

Fig. 8. Heat transfer coefficients vs. heat flux under vaporisation tests.

vaporisation tests, mass flux on refrigerant side G_r and water side G_w, heat flux Q/S. Table 3 also reports the maximum uncertainty for each variable.

Fig. 8 shows the refrigerant heat transfer coefficients during vaporisation tests against refrigerant heat flux. The "cross-grooved" surface and the roughened surface present similar heat transfer coefficients which are 30–40% higher than the smooth surface. The correlation between heat transfer coefficients and heat flux is well represented by a power-law function with an exponent from 0.5 (smooth surface) to 0.6 (roughened and "cross-grooved" surfaces), typical of nucleate boiling which, probably, is the dominant heat transfer regime in present vaporisation tests. Fig. 9 plots the heat transfer

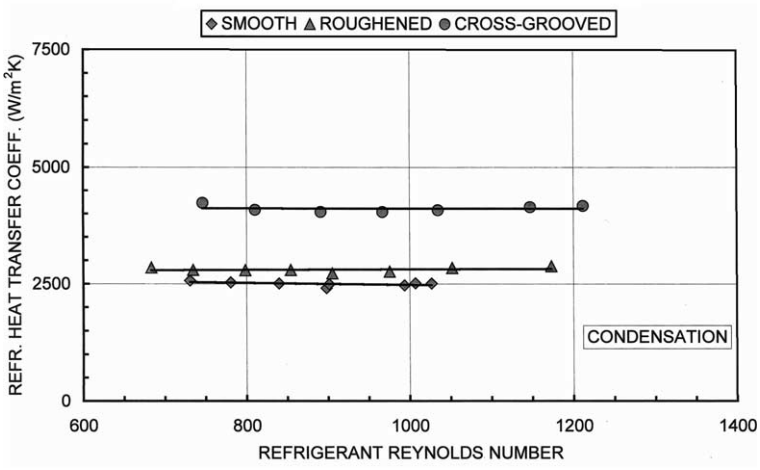

Fig. 9. Heat transfer coefficients vs. refrigerant Reynolds number under condensation tests.

coefficients during condensation tests against refrigerant Reynolds number. The "cross-grooved" surface presents heat transfer coefficients which are 50–60% higher than the roughened and the smooth surfaces respectively. It should be noted that during condensation tests the heat transfer coefficients are independent of refrigerant Reynolds number: therefore vapour shear forces have negligible effects on present condensation tests which are probably controlled by gravity forces.

The enhancement in heat transfer coefficients for the "cross-grooved" surface with respect to the smooth surface is higher than the simple increase in the heat transfer surface area (around 20%) both for vaporisation (30–40%) and condensation (60%). The increase over the simple heat transfer area enlargement is probably due to the enhancement in the nucleation sites density in the interfin spaces for vaporisation and to the effect of surface tension on condensate drainage for condensation.

Figs. 10 and 11 plot the total pressure drop during vaporisation and condensation tests against refrigerant Reynolds number. The roughened surface shows a pressure drop 10–20% higher than the "cross-grooved" surface and 20–40% higher than the smooth surfaces in vaporisation and condensation respectively. The condensation pressure drop data is more scattered than vaporisation data.

The "cross-grooved" surface presents a penalty in pressure drop with respect to the smooth surface, ranging from 10% to 20%, lower than the enhancement in heat transfer, which ranges from 30–40% in vaporisation to 60% in condensation. It should also be noted that during present experimental data the maximum

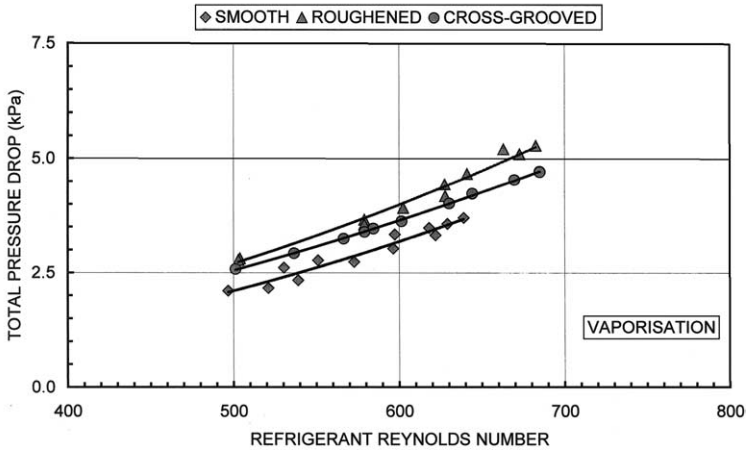

Fig. 10. Total pressure drop vs. refrigerant Reynolds number under vaporisation tests.

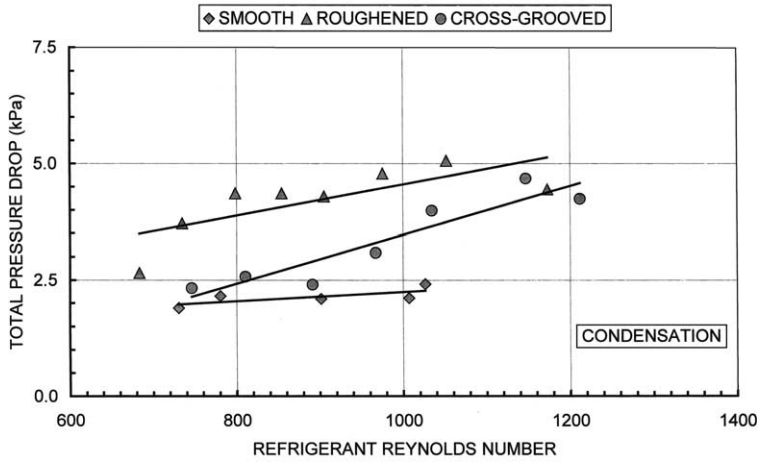

Fig. 11. Total pressure drop vs. refrigerant Reynolds number under condensation tests.

pressure drop measured on refrigerant side, around 5 kPa, involves a very small saturation temperature decrease, around 0.3 °C, with negligible effect on heat transfer, whereas the maximum pressure drop on the water side was lower than 40 kPa, a traditional design value for PHE water side.

The present experimental heat transfer coefficients were compared against semi-empirical correlations. Vaporisation data was compared against Cooper [15] equation and Gorenflo [16] correlation. Cooper equation, developed for nucleate boiling, accounts for heat flux, surface roughness and reduced pressure effects as follows:

$$h_r = 55P^{*(0.12-0.2\log_{10}R_p)}(-\log_{10}P^*)^{-0.55}q^{0.67}M^{-0.5} \quad (10)$$

where $P^* = P/P_{cr}$ is the reduced pressure, R_p (μm) is the roughness as defined in German standard DIN 4762/1, q (W m^{-2}) is the heat flux and M the molecular weight of the fluid. This correlation can process data relative to smooth and roughened surfaces: Fig. 12 shows the comparison between present experimental vaporisation data and the Cooper equation. The mean absolute percentage deviation is around 9%.

The Gorenflo correlation is valid for pool boiling and accounts for heat flux, surface roughness and reduced pressure effects as follows:

$$h_r = h_0 C_w F(P^*)(q/q_0)^n \quad (11)$$

where

$$h_0 = 3930\ \mathrm{W\,m^{-2}\,K^{-1}} \quad (12)$$

is the reference value ($P_0^* = 0.1$, $q_0 = 20000$ W m^{-2}, $R_{a0} = 0.4$ μm) of the heat transfer coefficient for refrigerant 22;

$$C_w = (R_a/0.4\ \mu\mathrm{m})^{0.1333} \quad (13)$$

accounts for the effect of the arithmetic mean roughness R_a (μm) of the surface as defined in ISO4287/1;

$$F(P^*) = 1.2P^{*0.27} + [2.5 + 1/(1 - P^*)]P^* \quad (14)$$

accounts for reduced pressure P^* effect;

$$(q/q_0)^n = (q/20000\ \mathrm{W\,m^{-2}})^{(0.9-0.3(P^*)^{\wedge 0.3})} \quad (15)$$

accounts for the heat flux q (W m^{-2}) effect. This correlation can be applied also to finned surface by using a proper value (experimental or theoretical) for the reference heat transfer coefficient h_0 and by modifying the correction factor for reduced pressure F and the exponent n of the correction factor for heat flux effect as follows:

$$F(P^*) = 1.2(P^*/\sqrt{\phi})^{0.27} + [2.5 + 1/(1 - (P^*/\sqrt{\phi}))](P^*/\sqrt{\phi}) \quad (16)$$

$$n = (0.9 - 0.3P^{*0.3}) - 0.1b/p \quad (17)$$

where ϕ is the ratio between finned and smooth surface areas, whereas b and p are fin height and pitch respectively. Fig. 13 shows the comparison between present experimental vaporisation data and the Gorenflo equation: the mean absolute percentage deviation is around 5%. The fair agreement with the Cooper and the Gorenflo correlations seems to confirm that present

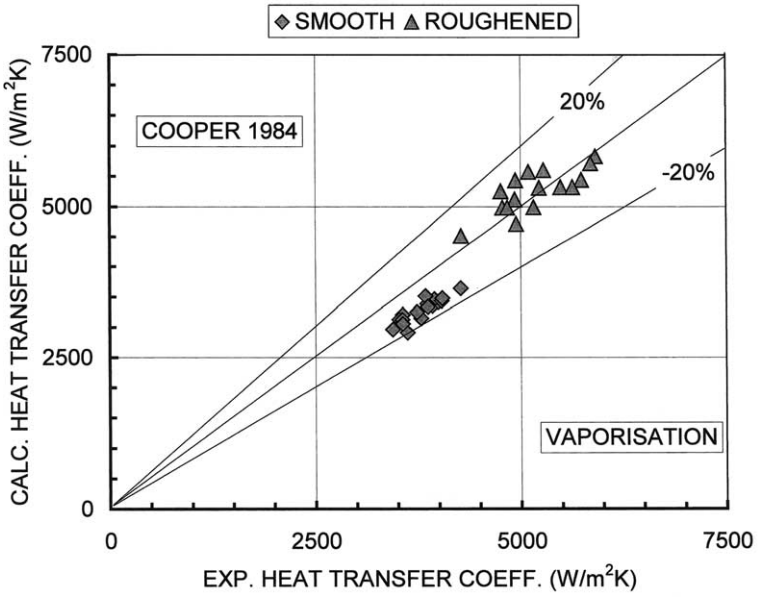

Fig. 12. Comparison between present vaporisation heat transfer coefficients and the Cooper [15] correlation.

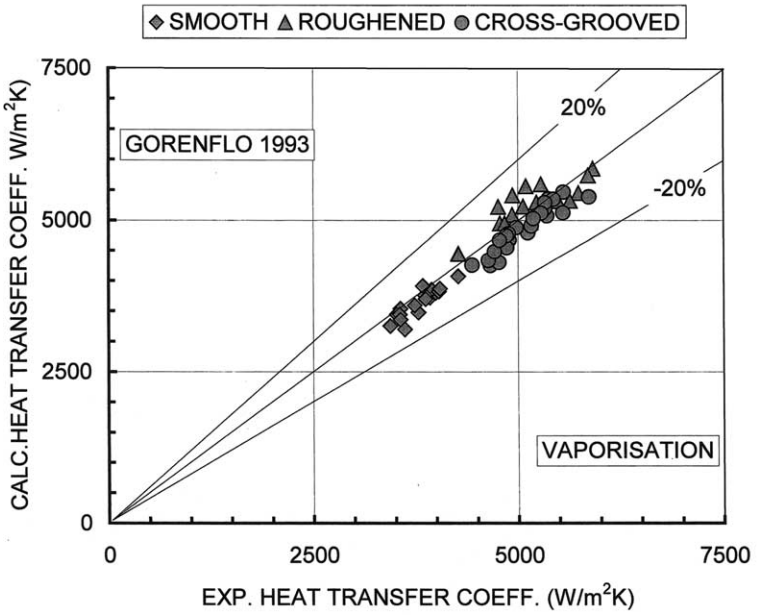

Fig. 13. Comparison between present vaporisation heat transfer coefficients and the Gorenflo [16] correlation.

vaporisation data is controlled by nucleate boiling. Condensation data was compared against the Yan et al. [4] model, a semi-empirical correlation based on a single set of R134a condensation data valid only for herringbone corrugation with an inclination angle around 60° and smooth and roughened surfaces:

$$h_r = 4.118(\lambda_L/d_h)Re_{eq}^{0.4}Pr_L^{1/3} \quad (18)$$

$$Re_{eq} = G[(1-x_m) + x_m(\rho_L/\rho_v)^{1/2}]d_h/\mu_L \quad (19)$$

$$Pr_L = \mu_L C_{pL}/\lambda_L \quad (20)$$

where x_m is the mean vapour quality. Fig. 14 shows the comparison between present experimental condensation data and Yan et al. equation: the mean absolute percentage deviation is around 11%. Condensation data

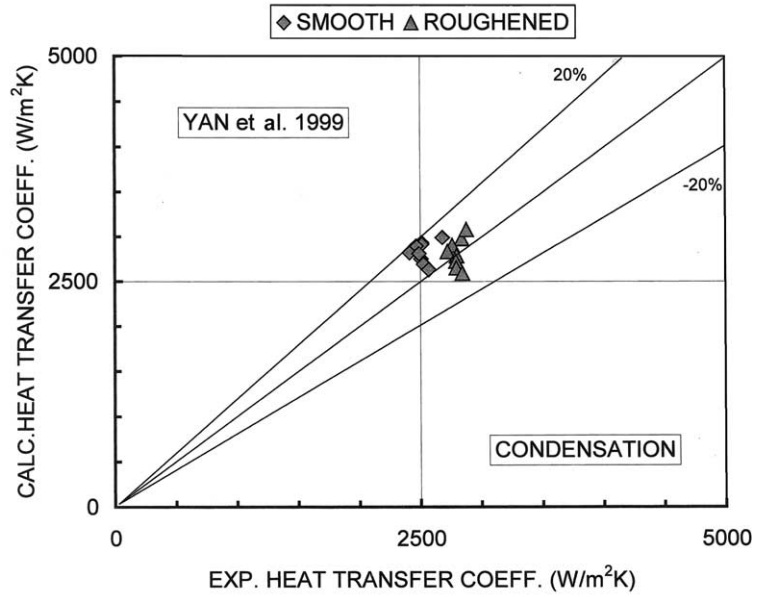

Fig. 14. Comparison between present condensation heat transfer coefficients and the Yan et al. [4] correlation.

was also compared against Nusselt's film theory [17] which underpredicts smooth surface data by about 41% and roughened surface data by about 46%. It is well known that Nusselt's theory generally also underpredicts condensation experimental data under gravity control as, in the real cases, the condensate does not flow as a uniform film under perfect laminar flow.

6. Conclusion

This paper presents the experimental work carried out to apply "cross-grooved" and roughened surfaces to refrigerant condensation and vaporisation inside herringbone-type PHE: more than 80 experimental data points were reported.

The "cross-grooved" surface is useful both in vaporisation and condensation giving an increase in the heat transfer coefficient on the refrigerant side from 30–40% in vaporisation to 60% in condensation with respect to a smooth surface.

The increase in surface roughness is useful only in vaporisation, giving a 30–40% increase in heat transfer coefficients with respect to a smooth surface.

The enhancement in heat transfer coefficient for "cross-grooved" surface with respect to smooth surface is higher than the simple increase in the heat transfer surface area and also greater than the penalty in pressure drop.

A critical aspect of this application, not discussed in the present paper, is the compatibility of the enhanced surfaces with the soldering process: in fact the "cross-grooved" surface or the roughened surface might be filled by soldering material during the brazing process. A patented technology [18] was developed to manufacture and solder the plates avoiding any damage to the enhanced surfaces.

References

[1] B. Thonon, R. Vidil, C. Marvillet, Recent research and developments in plate heat exchangers, J. Enhanced Heat Transfer 2 (1995) 149–155.

[2] B. Palm, B. Thonon, Thermal and hydraulic performances of compact heat exchangers for refrigeration systems, in: Proceedings of the International Conference on Compact Heat Exchangers and Enhancement Technology for the Process Industries, Banff, Canada, 1999, pp. 455–462.

[3] Y.Y. Yan, T.F. Lin, Evaporation heat transfer and pressure drop of refrigerant R-134a in a plate heat exchanger, ASME J. Heat Transfer 121 (1999) 118–127.

[4] Y.Y. Yan, H.C. Lio, T.F. Lin, Condensation heat transfer and pressure drop of refrigerant R-134a in a plate heat exchanger, Int. J. Heat Mass Transfer 42 (1999) 993–1006.

[5] Y.Y. Hsieh, T.F. Lin, Saturated flow boiling heat transfer and pressure drop of refrigerant R410A in a vertical plate heat exchanger, Int. J. Heat Mass Transfer 45 (2002) 1033–1044.

[6] H. Matsushita, M. Uchida, Evaporation performance of a plate heat exchanger embossed with pyramid-like structures, J. Enhanced Heat Transfer 9 (2002) 171–179.

[7] A. Cavallini, D. Del Col, L. Doretti, G.A. Longo, L. Rossetto, Enhanced intube heat transfer with refrigerants, in: Proceedings of 20th International Congress of Refrigeration, IIR/IIF, Sydney, Australia, 1999, Keynote Lecture, Paper no. 731.

[8] H.R. Engelhorn, A.M. Reihart, Investigations on heat transfer in plate evaporators, Chem. Eng. Process. 28 (1990) 143–146.

[9] T. Dutto, J.C. Blaise, T. Benedic, Performances of brazed plate heat exchanger set in heat pump, in: Proceedings of 18th International Congress of Refrigeration, Montreal, Canada, 1991, pp. 1284–1288.

[10] J. Claeson, B. Palm, Boiling mechanism in a small compact brazed plate heat exchanger (CBE) by using thermochromic liquid crystals (TLC), in: Proceedings of 20th International Congress of Refrigeration, Sydney, Australia, 1999, Paper no. 1177.

[11] R.K. Shah, W.W. Focke, Plate heat exchangers and their design theory, in: Heat Transfer Equipment Design, Hemisphere, Washington, 1988, pp. 227–254.

[12] A. Muley, R.M. Manglik, Experimental study of turbulent flow heat transfer and pressure drop in a plate heat exchanger with chevron plates, ASME J. Heat Transfer 121 (1999) 110–121.

[13] NIST, The US National Institute of Standards and Technology, Refrigerant properties computer code, REFPROP 6.1, 2001.

[14] S.J. Kline, F.A. McClintock, Describing uncertainties in single-sample experiments, Mech. Eng. 75 (1953) 3–8.

[15] M.G. Cooper, Heat flows rates in saturated pool boiling—A wide ranging examination using reduced properties, in: Advanced in Heat Transfer, Academic Press, Orlando, FL, 1984.

[16] D. Gorenflo, Pool Boiling, VDI Heat Atlas, Dusseldorf, Germany, 1993, Hal-25.

[17] W. Nusselt, Die oberfiachenkondensation des wasserdampfes, Z. Ver. Dt. Ing. 60 (1916) 541–546, 569–575.

[18] Plate heat exchanger, European Patent EP 1394 491 A.